Available online at www.sciencedirect.com

ScienceDirect

Procedia IUTAM 19 (2016) 236 – 243

Procedia IUTAM

www.elsevier.com/locate/procedia

IUTAM Symposium Analytical Methods in Nonlinear Dynamics

# Discrete breathers in forced chains of oscillators with cubic nonlinearities

Francesco Romeo[a,*], Oleg V. Gendelman[b]

[a]*Sapienza University of Rome, Via Gramsci 53, Rome 00197, Italy*
[b]*Technion - Israel Institute of Technology, Technion City, Haifa 3200003, Israel*

**Abstract**

The forced dynamics of chains of linearly coupled mechanical oscillators characterized by on-site cubic nonlinearity is investigated. The study aims to highlight the role played by the harmonic excitation on the nonlinear spatially localised dynamics of the system. Towards this goal, a map approach is employed in order to identify the chain nonlinear propagation regions under 1:1 resonance conditions. Given the latter assumption, the governing second-order difference equation refers to a perturbation of the stationary resonant response. Softening and hardening type of nonlinearities are considered and the associated unstaggered and staggered discrete breathers (DB), respectively, are discussed. Stationary DBs obtained as soliton-like solutions are identified either with sequences of the nonlinear map homoclinic primary intersection points and with an ad hoc analytic approximation; the latter is based on the idea that the nonlinearity is taken into account only in the central part of the breather whilst the tails are treated as linear excitations.


Peer-review under responsibility of organizing committee of IUTAM Symposium Analytical Methods in Nonlinear Dynamics

*Keywords:* Discrete breathers; nonlinear oscillatory chains.

## 1. Introduction

Localization phenomena are ubiquitous in nonlinear dynamical systems. One of the most important and widely studied localization-related effects is appearance of spatially localized, time periodic solutions, which are referred to as discrete breathers (DB) or intrinsic localized modes (ILM). Such partial solutions were revealed in many mechanical models, such as micromechanical cantilever arrays[1,2], chains of coupled pendula[3] and chains with vibro-impact constraints[4]. While the experimental evidences primarily refer to forced/damped chains, most theoretical studies concern with unforced chains. For the latter case, different computational and analytical approaches are indeed available[5]. By addressing chains of linearly coupled mechanical oscillators with cubic nonlinear stiffness, a two-fold purpose is pursued in this study: to extend the map approach, so far limited to free dynamics[6,7,8], to forced nonlinear chains and to validate the localized solutions obtained through an approximate analytical approach[9] by comparing them with the solutions obtained through the map approach. As far as the unforced chains, the map based geometric approach

* Corresponding author. Tel.: +39-06-49919235 ; fax: +39-06-49919192.
*E-mail address:* francesco.romeo@uniroma1.it


Peer-review under responsibility of organizing committee of IUTAM Symposium Analytical Methods in Nonlinear Dynamics
doi:10.1016/j.piutam.2016.03.030

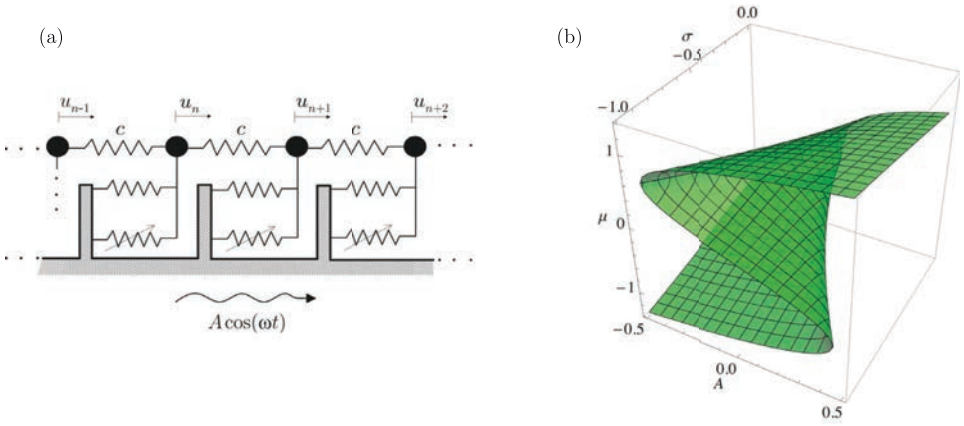


Fig. 1. (a) Schematic view of the forced nonlinear oscillatory chain; (b) surface described by the roots $\mu$ of eq. (4).

allows to identify bright (dark) DBs with sequences of homoclinic (heteroclinic) intersection points of the nonlinear mapping. Being in this study interested only in the bright ones, the attention will be focused on the influence of the forcing amplitude on the unstable fixed points as they govern the DBs existence since stable and unstable manifolds emanate from them. In particular, the interest lies in the case in which the trivial solution is hyperbolic, namely outside the linear passing band, where the existence of unstaggered (staggered) bright DBs associated to softening (hardening) nonlinearity was already evidenced by the free dynamics analysis of the chain. Besides few exceptions, closed analytic forms for breather solutions in damped forced chains are not available. However, there is a vast body of literature proposing approximations to exact breather solutions, such as those based on rotating-waves, multiple scale expansion and harmonic balance. The approximation proposed in this work is based on the idea that the nonlinearity is taken into account only in the central part of the breather while the tails are treated as linear excitations. This procedure, based on harmonic balance method, allows drastic reduction of the dimensionality and allows one to obtain tractable analytic expressions for predicting the existence of a DB under a specific set of parameters.

A forced chain of linearly coupled nonlinear oscillators, sketched in Fig. 1a, is studied by considering the dynamics of the generic $n$-th oscillator, governed by the following equation of motion [10]

$$\ddot{u}_n + u_n \pm u_n^3 + c(2u_n - u_{n-1} - u_{n+1}) = A\cos\omega t \tag{1}$$

where $c$ represents the linear coupling stiffness. The harmonic forcing amplitude and frequency are given by $A$ and $\omega$, respectively, and either positive (hardening) and negative (softening) cubic term is considered. Time periodic solutions of equation (1) are sought for by assuming the harmonic solution $u_n = a_n\cos(\omega t)$. Equating coefficients of $\cos(\omega t)$, thereby assuming 1:1 resonance conditions, gives

$$(1-\omega^2)a_n \pm \frac{3}{4}a_n^3 + c(2a_n - a_{n-1} - a_{n+1}) = A \tag{2}$$

Willing to describe the motion of a perturbation of the underlying stationary resonant response, we set $a_n = \gamma_n + \mu$, then, by setting $1-\omega^2 = \sigma$, equation (2) becomes

$$\sigma(\gamma_n + \mu) \pm \frac{3}{4}(\gamma_n + \mu)^3 + c(2\gamma_n - \gamma_{n-1} - \gamma_{n+1}) = A \tag{3}$$

The cubic nonlinearity allows to set

$$\sigma\mu \pm \frac{3}{4}\mu^3 = A \tag{4}$$

Among the real roots $\mu_i$, i= 1, 2, 3 of Eq. (4), located on the surface represented in Fig. 1b, the ones corresponding to stable solutions are selected and substituted into the map

$$\alpha\gamma_n \mp \beta(\gamma_n^3 + 3\gamma_n^2\mu + 3\gamma_n\mu^2) + \gamma_{n-1} + \gamma_{n+1} = 0 \tag{5}$$

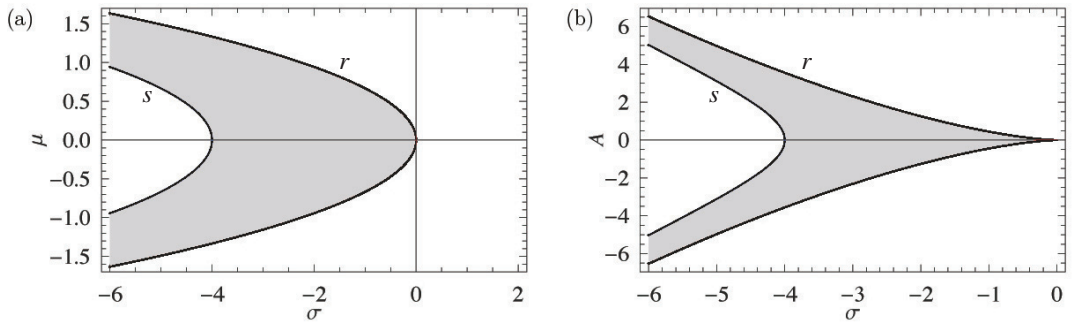


Fig. 2. Propagation regions on the $\sigma - \mu$ (a) and $\sigma - A$ (b) planes for $\gamma_n = 0$ and $c = 1$ (hardening case). The boundaries $r$ and $s$ correspond to the conditions $tr(\mathbf{DT}) = \pm 2$, respectively.

where $\alpha = -\frac{\sigma}{c} - 2$ , $\beta = \frac{3}{4c}$. As known, the frequency dependent nonlinear map defined by (5), in which the positive (negative) sign corresponds to hardening (softening) nonlinearity, belongs to the class of area preserving maps such that $\det(\mathbf{DT}(\gamma_n, \mu)) = 1$, where $\mathbf{DT}$ is the Jacobian or tangent map with reciprocal eigenvalues [8]:

$$\mathbf{DT} = \begin{bmatrix} -\alpha \pm \beta(3\gamma_n^2 + 6\gamma_n\mu + 3\mu^2) & -1 \\ 1 & 0 \end{bmatrix} \tag{6}$$

From the conditions $|tr(\mathbf{DT})| = 2$, with the positive (negative) sign for the hardening (softening) nonlinearity and $\gamma_n = 0$ and $c = 1$, the boundaries of the nonlinear propagation regions shown in Fig. 2 are obtained. Therefore, at first, the map dependence on the underlying stationary amplitude is neglected and the dependence of the propagation regions on the excitation amplitude is described. In particular, these regions are represented on both the $\sigma - \mu$ (Fig. 2a) and the $\sigma - A$ (Fig. 2b) planes. The projection on the $\mu - \sigma$ plane of the propagation zone boundaries are given by $r(\sigma) = \pm i\sqrt{\frac{\sigma}{3\beta}}$, $s(\sigma) = \pm\sqrt{\frac{-4-\sigma}{3\beta}}$. The two curves $r$, $s$ represent hyperbolic ($\lambda_1 = \lambda_2 = 1$) and reflection hyperbolic ($\lambda_1 = \lambda_2 = -1$) thresholds, respectively.

## 2. Nonlinear propagation regions and map invariant manifolds

The existence of stationary bright DBs is strictly linked to the nature of the nonlinear map (5) fixed points. The latter can be determined by merging the information gathered from the nonlinear propagation region on the $\sigma - \mu$ plane and the invariant manifolds. As usually done for 2D real maps, by setting $\gamma_{n+1} = x_{n+1}$ and $\gamma_n = y_{n+1}$, these manifolds can be represented on the $x - y$ plane.

As shown in Fig. 3 for the softening case with $\sigma = 0.7$ (Fig. 3a), the presence of the forcing term alters the position of the fixed points along the symmetry line $x = y$ (Fig. 3b,c,d). In essence, as the forcing amplitude level increases, the stable fixed points (green dots in Fig. 3b,c,d) are no longer symmetric with respect to $x = -y$. Outside the propagation regions (e.g. points B,C in Fig. 3a), the fixed points $(0, 0)$ are hyperbolic and the homoclinic invariant manifolds can emanate from them (red dots in Fig. 3b,c). Differently, by entering the bounded region through the boundary $r$ (e.g. point D in Fig. 3), the fixed points $(0, 0)$ become elliptic and the unstable ones move along the main symmetry line $x = y$ (see Fig. 3c). Further increase of $\mu$ will eventually lead such unstable fixed point to coalesce with the lower stable fixed point and the homoclinic scenario vanishes.

The corresponding evolution of the invariant manifolds for the hardening case with $\sigma = -4.3$ is shown in Fig. 4. The homoclinic tangle is here organized along the symmetry line $x = -y$ and it is surrounded by an heteroclinic one governed by two period-1 unstable solutions (located along the symmetry line $x = y$). In this case, as $\mu$ increases, the homoclinic tangle shrinks until the two stable fixed points, at the boundary $s$ crossing, coalesce with the unstable one at the origin. Therefore the latter fixed point becomes stable until further increase of $\mu$ leads out of the propagation region through the boundary $r$ after which one of the upper unstable fixed point, located on the symmetry axis $x = y$,

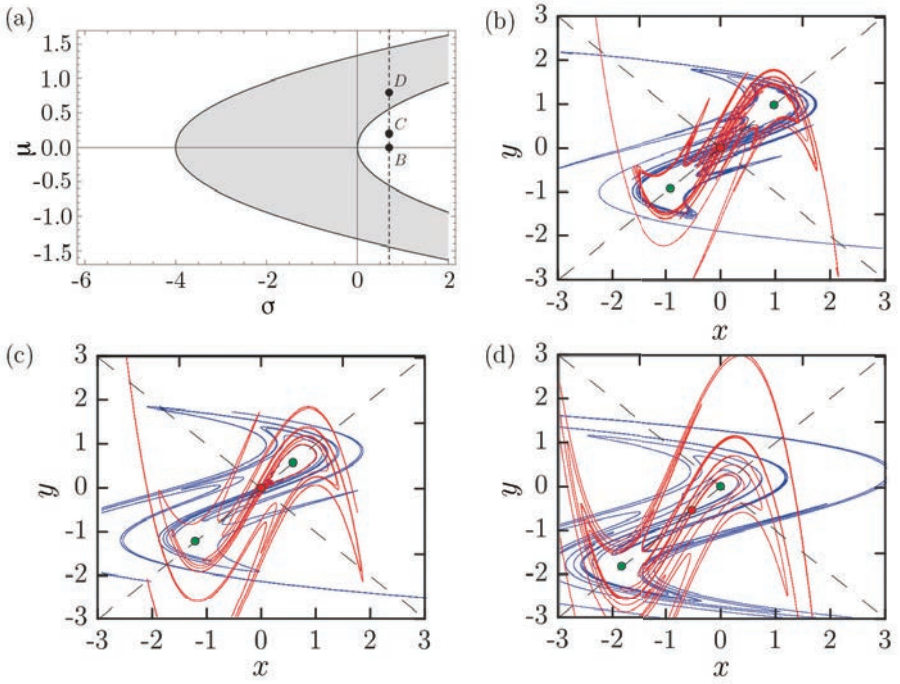


Fig. 3. Propagation region (a) and invariant manifolds scenarios (b,c,d) for increasing forcing amplitude level and $\sigma = 0.7$ (softening); stable (blue) and unstable (red) manifolds and fixed points (red: hyperbolic, green: elliptic): b) $\mu = 0.0\,(A = 0.0)$, point B; c) $\mu = 0.2\,(A = -0.93)$, point C; d) $\mu = 0.8\,(A = -3.38)$, point D.

coalesces with the origin that becomes unstable. The remaining heteroclinc tangle lasts until the stable fixed point reaches the lower unstable one.

## 3. Discrete breathers as homoclinic orbits

Stationary discrete breathers, i.e. time-periodic spatially localized solutions, are solutions with period $T_b = 2\pi/\Omega_b$, that can be expanded in a Fourier series as follows[5]

$$u_n(t) = \sum_j a_{jn} e^{ij\Omega_b t}, \quad a_{j,|n|\to\infty} \to 0 \tag{7}$$

where the Fourier coefficients are assumed localized in space. We look for such localized states by relating them to the intersections of the invariant manifolds emanating from unstable fixed points of the map. In particular, we consider the single mode approximation, namely $j = 1$. A point belonging to $\mathcal{W}^s(P)$ ($\mathcal{W}^u(P)$) approaches $P$ under map iteration $\mathbf{T}^n$ for $n \to \infty$ ($n \to -\infty$). A homoclinic point $Q$ is defined as $Q \in \mathcal{W}^s \cap \mathcal{W}^u$; thus, any $Q$ belongs to both the stable and unstable manifold of $P$ so, when iterated either forward or backward, it will converge to $P$ and it corresponds to a breather solution.

## 4. Analytical approach and discrete breathers comparison

Exact analytical approaches for the analysis of DB are seldom available[4]. The DB map-based analysis is compared with an analytic approach based on a single particle DB approximation and harmonic balance method[9]. The prediction of DB existence zone in the space of parameters provided by the two approaches is eventually discussed.

From

$$(1 - \omega^2)a_n \pm \frac{3}{4}a_n^3 + c(2a_n - a_{n-1} - a_{n+1}) = A \tag{8}$$

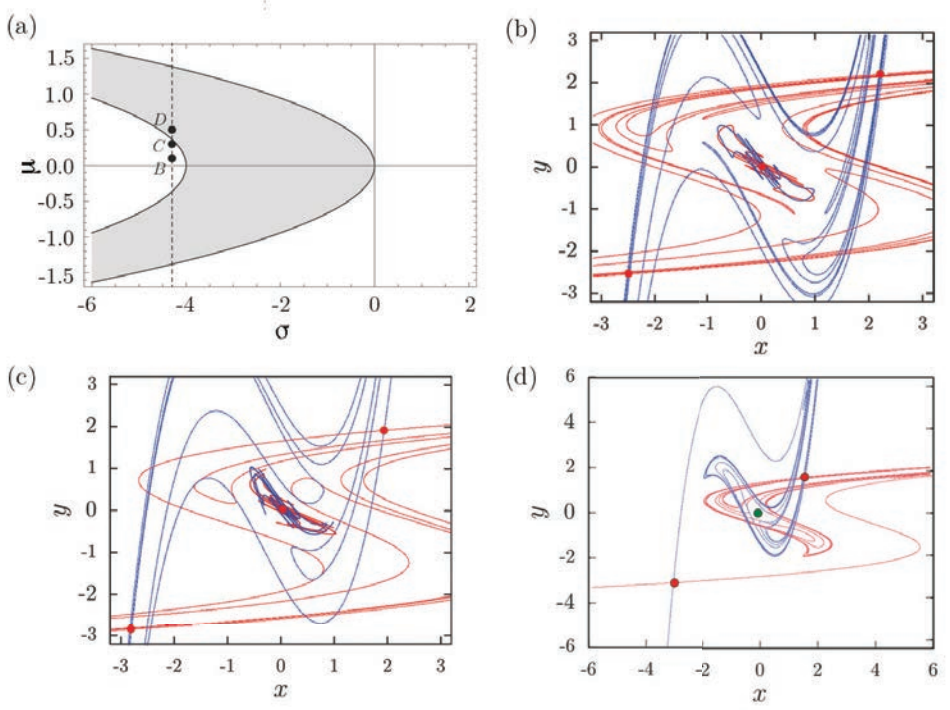


Fig. 4. Propagation region (a) and invariant manifolds scenarios (b,c,d) for increasing forcing amplitude level and $\sigma = -4.3$ (hardening); stable (blue) and unstable (red) manifolds and fixed points (red: hyperbolic, green: elliptic): b) $\mu = 0.1$ ($A = -0.43$) point B; c) $\mu = 0.3$ ($A = -1.29$), point C; d) $\mu = 0.5$ ($A = -2.15$), point D.

By introducing the basic assumption according to which the nonlinearity is taken into account only for the site $n = 0$, then, for sites with $n \neq 0$, we can put

$$(1 - \omega^2)a_n + c(2a_n - a_{n-1} - a_{n+1}) = A \tag{9}$$

Eq. (9) is solved (separately for $n > 0$ and $n < 0$, these solutions being symmetric) as follows:

$$a_n = \frac{A}{1 - \omega^2} + (\mp 1)^n \varphi_0 q^{|n|}\,, \; n \neq 0 \tag{10}$$

$$q = \pm\frac{\omega^2 - 1}{2c} \mp 1 - \sqrt{\frac{(\omega^2 - 1)^2}{4c^2} - \frac{\omega^2 - 1}{c}} \tag{11}$$

For the centered (zero) site, we have:

$$a_0 = \frac{A}{1 - \omega^2} + \varphi_0 \tag{12}$$

$$(1 - \omega^2)\left(\frac{A}{1 - \omega^2} + \varphi_0\right) \pm \frac{3}{4}\left(\frac{A}{1 - \omega^2} + \varphi_0\right)^3 + 2c\varphi_0(1 \pm q) = A \tag{13}$$

Simplifying and using expression (11) for $q$, we obtain the following cubic equation for $\varphi_0$

$$\frac{3}{4}\left(\frac{A}{1 - \omega^2} + \varphi_0\right)^3 - \varphi_0\sqrt{(\omega^2 - 1)^2 - 4c(\omega^2 - 1)} = 0 \tag{14}$$

From the solutions of the cubic equation in $\varphi_0$ (14), the region of existence of the DBs can be derived. In particular, if the cubic equation in $\varphi_0$ has three real solutions, then the breather solution exists and the largest root corresponds to

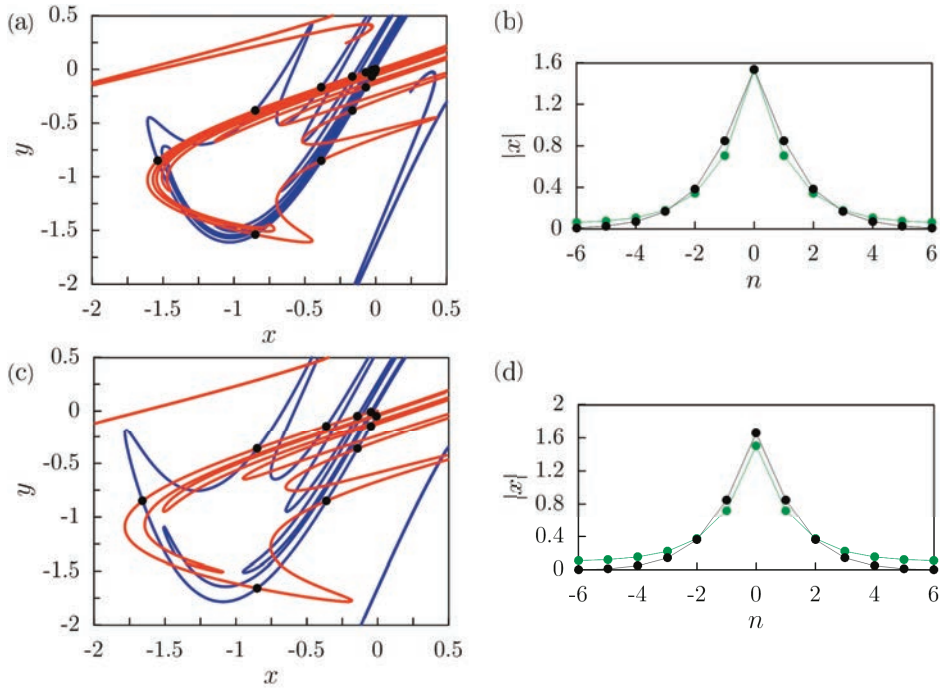


Fig. 5. Stable (blue) and unstable (red) manifolds and primary intersections (black dots) for $\sigma = 0.7$: a) $\mu = 0.05$; c) $\mu = 0.1$. Unstaggered DB corresponding to the homoclinic orbit of $(0, 0)$ (black) and single particle DB approximation (green): b) $\mu = 0.05$; d) $\mu = 0.1$.

the breather amplitude. Depending on the sign of the cubic nonlinear term we distinguish two cases. *Hardening*: The staggered breathers corresponding to the homoclinic orbits exist only in the 'left' attenuation zone, so for $\omega^2 > 1 + 4c$ ($\sigma < -4$) and $0 < q < 1$. *Softening*: The unstaggered breathers corresponding to the homoclinic orbits exist only in the 'right' attenuation zone, so for $\omega < 1$ ($\sigma > 0$) and $0 < q < 1$. The exponential convergence to the saddle is provided by $q^n$ while the parametric relation $\mu = \frac{A}{1-\omega^2}$ allows to compare the DBs obtained through the analytic approximation and those obtained through the map approach. As far as the softening case ($\sigma = 0.7$), the results presented in Fig. 5a,b refer to the value $\mu = 0.05$ ($\varphi_{0,1} = -1.629, \varphi_{0,2} = 5.2 \times 10^{-5}, \varphi_{0,3} = 1.479$) while those presented in Fig. 5c,d refer to $\mu = 0.1$ ($\varphi_{0,1} = -1.703, \varphi_{0,2} = 0.00042, \varphi_{0,3} = 1.402$). According to the analytical prediction, the case $\mu = 0.8$ provides the complex roots $\varphi_{0,1} = -2.659, \varphi_{0,2} = 0.13 + 0.419i, \varphi_{0,3} = 0.13 - 0.419i$. Figures 5a,c show the stable (blue) and unstable (red) manifolds emanating from the unstable fixed point at the origin together with the primary intersection points for $\mu = 0.05$ and $\mu = 0.1$, respectively. The corresponding homoclinic orbits (black) are shown in Figs. 5b,d where they are compared with the DB analytical approximation (green). As expected, the good agreement observed for low values of $\mu$ in terms of both central peak value and exponential decay gets worse as $\mu$ and the DBs peak amplitude increases. For the hardening case ($\sigma = -4.3$), the results are reported in Fig. 6; in particular, Figs. 6a,b correspond to the value $\mu = 0.1$ ($\varphi_{0,1} = -1.377, \varphi_{0,2} = 0.00067, \varphi_{0,3} = 1.077$) while figures 6c,d refer to the case $\mu = 0.2$ ($\varphi_{0,1} = -1.520, \varphi_{0,2} = 0.006, \varphi_{0,3} = 0.95$). Also in this case inside the propagation region, e.g. for $\mu = 0.5$, complex roots are found ($\varphi_{0,1} = -1.929, \varphi_{0,2} = 0.215 + 0.136i, \varphi_{0,3} = 0.215 - 0.136i$). The agreement between the homclinic orbits (black) and the corresponding analytical approximation (green) is shown in figures 6b,d. In this case the approximation of the DB peak amplitude for $\mu = 0.2$ is more accurate than for $\mu = 0.1$; this trend can be explained by noticing that, differently form the previous softening (unstaggered) case, in the hardening (staggered) case the homoclinic tangle, and therefore the DBs peak amplitude, shrinks (see figure 4b,c,d) as $\mu$ increases.

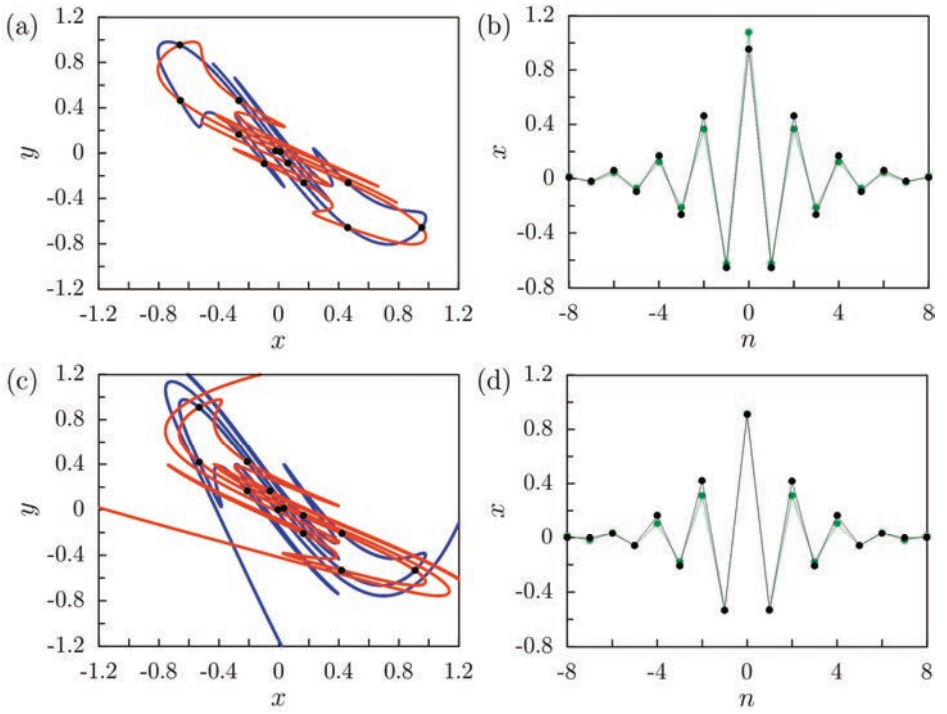


Fig. 6. Stable (blue) and unstable (red) manifolds and primary intersections (black dots) for $\sigma = -4.3$: a) $\mu = 0.1$; c) $\mu = 0.2$. Staggered DB corresponding to the homoclinic orbit of $(0, 0)$ (black) and single particle DB approximation (green): b) $\mu = 0.1$; d) $\mu = 0.2$.

## 5. Conclusions

The nonlinear propagation regions and invariant manifolds of a forced oscillatory chain were derived through a map approach; guided by these regions, the zones of existence of homoclinic orbits and corresponding discrete breathers were identified. The stability of the map's trivial fixed points depends on the forcing amplitude, moreover, as the forcing amplitude level increases, the stable fixed points are no longer symmetrically located with respect to the main symmetry lines. For the considered weakly nonlinear linearly coupled oscillators, the analytical approximation based on a DB concentrated primarily on a single particle provided satisfactory initial results. The agreement between the analytic approximation and the map homoclinic orbits improves as the peak amplitude of DBs decreases. Thus the best accuracy is obtained in the neighborhood of the propagation regions boundaries. Further developments will aim to address the stability of the obtained DBs, to tackle more general classes of DBs (i.e. dark breathers, multibreathers) and to consider dissipative chains.

## Acknowledgements

The authors are grateful to Israel Science Foundation (grant 838/13) for financial support.

## References

1. Sato M, Hubbard BE, Sievers AJ. Nonlinear energy localization and its manipulation in micromechanical oscillator arrays. *Rev Modern Phys* 2006; **78**:137-157.
2. Sato M, Sievers AJ. Driven localized excitations in the acoustic spectrum of small nonlinear macroscopic and microscopic lattices. *Phys Rev Lett* 2007; **98**:214101.
3. Cuevas J, English LQ, Kevrekidis PG, and Anderson M. Discrete breathers in a forced-damped array of coupled pendula: Modeling, computation, and experiment. *Phys Rev Lett* 2009; **102**:224101.

4. Gendelman O. Exact solutions for discrete breathers in a forced-damped chain. *Phys Rev E* 2013; **87**:062911.
5. Flach S, Gorbach AV. Discrete breathers Advances in theory and applications. *Phys Reports* 2008; **467**:1-116.
6. Hennig D, Rasmussen K, Gabriel H and Blow A. Soliton-like solutions of the generalized discrete nonlinear Schrödinger equation. *Phys Rev E* 1996; **54**:5788-5801.
7. Bountis T, Capel HW, Kollmann M, Ross JC, Bergamin JM, van der Weele JP. Multibreathers and homoclinic orbits in 1-dimensional nonlinear lattices. *Phys. Lett. A* 2000; **268**:50-60.
8. Romeo F, Rega G. Periodic and localized solutions in chains of oscillators with softening or hardening cubic nonlinearity. *Meccanica* 2015; **50**:721-730.
9. Veremkroit M. Analytic Exploration of Discrete Breathers in a Forced-Damped Klein-Gordon type Chain. Master Thesis, Technion - Israel Institute of Technology, 2014.
10. Umberger KD, Grebogi C, Ott E, Afeyan B Spatiotemporal dynamics in a dispersively coupled chain of nonlinear oscillators. *Phys. Rev. A* 1989; **39**:483542.